

Observation of an anomalous positron abundance in the cosmic radiation

O. Adriani,^{1,2} G. C. Barbarino,^{3,4} G. A. Bazilevskaya,⁵ R. Bellotti,^{6,7} M. Boezio,⁸ E. A. Bogomolov,⁹ L. Bonechi,^{1,2} M. Bongi,² V. Bonvicini,⁸ S. Bottai,² A. Bruno,^{6,7} F. Cafagna,⁷ D. Campana,⁴ P. Carlson,¹⁰ M. Casolino,¹¹ G. Castellini,¹² M. P. De Pascale,^{11,13} G. De Rosa,⁴ N. De Simone,^{11,13} V. Di Felice,^{11,13} A. M. Galper,¹⁴ L. Grishantseva,¹⁴ P. Hofverberg,¹⁰ A. Leonov,¹⁴ S. V. Koldashov,¹⁴ S. Y. Krutkov,⁹ A. N. Kvashnin,¹⁵ V. Malvezzi,¹¹ L. Marcelli,¹¹ W. Menn,¹⁶ V. V. Mikhailov,¹⁴ E. Mocchiutti,⁸ S. Orsi,¹⁰ G. Osteria,⁴ P. Papini,² M. Pearce,¹⁰ P. Picozza,^{11,13} M. Ricci,¹⁷ S. B. Ricciarini,² M. Simon,¹⁶ R. Sparvoli,^{11,13} P. Spillantini,^{1,2} Y. I. Stozhkov,¹⁵ A. Vacchi,⁸ E. Vannuccini,² G. Vasilyev,⁹ S. A. Voronov,¹⁴ Y. T. Yurkin,¹⁴ G. Zampa,⁸ N. Zampa,⁸ and V. G. Zverev¹⁴

¹*Physics Department of University of Florence,
I-50019 Sesto Fiorentino, Florence, Italy*

²*INFN, Sezione di Florence, I-50019 Sesto Fiorentino, Florence, Italy*

³*Physics Department of University of Naples "Federico II", I-80126 Naples, Italy*

⁴*INFN, Sezione di Naples, I-80126 Naples, Italy*

⁵*Lebedev Physical Institute, Leninsky Prospekt 53, RU-119991 Moscow, Russia*

⁶*Physics Department of University of Bari, I-70126 Bari, Italy*

⁷*INFN, Sezione di Bari, I-70126 Bari, Italy*

⁸*INFN, Sezione di Trieste, I-34012 Trieste, Italy*

⁹*Ioffe Physical Technical Institute, RU-194021 St. Petersburg, Russia*

¹⁰*Physics Department of the Royal Institute of
Technology (KTH), SE-10691 Stockholm, Sweden*

¹¹*INFN, Sezione di Rome "Tor Vergata", I-00133 Rome, Italy*

¹²*IFAC, I-50019 Sesto Fiorentino, Florence, Italy*

¹³*Physics Department of University of Rome "Tor Vergata", I-00133 Rome, Italy*

¹⁴*Moscow Engineering and Physics Institute, RU-11540 Moscow, Russia*

¹⁵*Lebedev Physical Institute, RU-119991 Moscow, Russia*

¹⁶*Physics Department of Universität Siegen, D-57068 Siegen, Germany*

¹⁷*INFN, Laboratori Nazionali di Frascati,*

Via Enrico Fermi 40, I-00044 Frascati, Italy

(Dated: October 28, 2008)

Abstract

Positrons are known to be produced in interactions between cosmic-ray nuclei and interstellar matter (“secondary production”). Positrons may, however, also be created by dark matter particle annihilations in the galactic halo or in the magnetospheres of near-by pulsars. The nature of dark matter is one of the most prominent open questions in science today. An observation of positrons from pulsars would open a new observation window on these sources. Here we present results from the PAMELA satellite experiment on the positron abundance in the cosmic radiation for the energy range 1.5 - 100 GeV. Our high energy data deviate significantly from predictions of secondary production models, and may constitute the first indirect evidence of dark matter particle annihilations, or the first observation of positron production from near-by pulsars. We also present evidence that solar activity significantly affects the abundance of positrons at low energies.

Measurements of cosmic-ray positrons (e^+) and electrons (e^-) address a number of questions in contemporary astrophysics, such as the nature and distribution of particle sources in our galaxy, and the subsequent propagation of cosmic-rays through the galaxy and the solar magnetosphere. Positrons are believed to be mainly created in secondary production processes resulting from the interaction of cosmic-ray nuclei with the interstellar gas. A ratio of positron and electron fluxes (ϕ), the positron fraction, $\phi(e^+) / (\phi(e^+) + \phi(e^-))$, can be used to investigate possible primary sources. If secondary production dominates, the positron fraction is expected to fall as a smooth function of increasing energy.

The energy budget of the Universe can be broken down into baryonic matter (about 5%), dark matter (about 23%) and dark energy (about 72%) (e.g.[1]). Many particle candidates have been proposed for the dark matter component. The most widely studied are the neutralino from supersymmetric models (e.g.[2]) and the lightest Kaluza Klein particle from extra dimension models (e.g.[3]). The gravitino (e.g.[4]) is also an interesting candidate. High energy antiparticles such as positrons[5, 6, 7, 8, 9, 10, 11, 12, 13] and antiprotons[2, 14] can be produced during the annihilation or decay of these dark matter particles in our galaxy. In a previous publication[15] we presented the antiproton-to-proton flux ratio in the energy range 1-100 GeV. The data follow the trend expected from secondary production calculations for antiprotons and place significant constraints on contributions to the antiproton flux from dark matter particle annihilations. The possible production of positrons from nearby astrophysical sources, such as pulsars[16, 17, 18, 19, 20], must be taken into account when interpreting potential dark matter signals.

Cosmic-ray positrons and electrons have been studied mainly by balloon-borne instruments with correspondingly short observation times, and significant atmospheric overburden (for a review see[21]). Their results show large discrepancies, especially at high energies (above 10 GeV). This high energy region is the most interesting since the poorly understood modulation of particle fluxes by the solar wind has no relevant effect and possible signatures of primary components should be most evident. Although too statistically limited to draw any significant conclusions, the most recent high energy measurements[22, 23, 24] indicate a flatter positron fraction than expected from secondary production models.

ELECTRON AND POSITRON IDENTIFICATION

The PAMELA[25] apparatus is a system of electronic particle detectors optimised for the study of antiparticles in the cosmic radiation. It was launched from the Bajkonur Cosmodrome on June 15th 2006 on-board a satellite that was placed into a 70.0° inclination orbit, at an altitude varying between 350 km and 610 km. Electrons and positrons can be reliably distinguished from the other cosmic-ray species impinging on PAMELA (mostly protons) by combining information provided by the different detector components. A permanent magnet spectrometer with a silicon tracking system allows the rigidity (momentum / charge, here in units of GV), and sign-of-charge of the incident particle to be determined. The interaction pattern in a imaging silicon-tungsten calorimeter allows electrons and positrons to be separated from protons.

The misidentification of electrons and, in particular, protons is the largest source of background when estimating the positron fraction. This can occur if the sign-of-charge is incorrectly assigned from the spectrometer data, or if electron- and proton-like interaction patterns are confused in the calorimeter data. The antiproton-to-electron flux ratio in the cosmic radiation is approximately 10^{-2} between 1 and 100 GV but can be reduced to a negligible level after electrons are selected using calorimeter information. The proton-to-positron flux ratio, however, increases from approximately 10^3 at 1 GV to approximately 10^4 at 100 GV. Robust positron identification is therefore required, and the residual proton background must be estimated accurately. The imaging calorimeter is 16.3 radiation lengths (0.6 nuclear interaction lengths) deep, so electrons and positrons develop well contained electromagnetic showers in the energy range of interest. In contrast, the majority of the protons will either pass through the calorimeter as a minimum ionising particle or interact deep in the calorimeter. Particle identification based on the total measured energy and the starting point of the reconstructed shower in the calorimeter can be tuned to reject 99.9% of the protons, while selecting $> 95\%$ of the electrons or positrons. The remaining proton contamination in the positron sample can be eliminated using additional topological information, including the lateral and longitudinal profile of the shower. Using particle beam data collected at CERN we have previously shown[26] that less than one proton out of 100,000 passes the calorimeter electron selection up to 200 GeV/c, with a corresponding electron selection efficiency of 80%.

To illustrate this approach, Fig. 1 shows \mathcal{F} , the fraction of calorimeter energy deposited inside a cylinder of radius 0.3 Molière radii, as a function of deflection (rigidity⁻¹). The axis of the cylinder is defined by extrapolating the particle track reconstructed in the spectrometer. The Molière radius is an important quantity in calorimetry as it quantifies the lateral spread of an electromagnetic shower (about 90% of the shower energy is contained in a cylinder with a radius equal to 1 Molière radius), and depends only on the absorbing material (tungsten in this case). The events shown in Fig. 1 were selected requiring a match between the momentum measured by the tracking system and the total detected energy and the starting point of the shower in the calorimeter. For negatively-signed deflections, electrons are clearly visible as a horizontal band with \mathcal{F} lying mostly between 0.4 and 0.7. For positively-signed deflections, the similar horizontal band is naturally associated to positrons, with the remaining points, mostly at $\mathcal{F} < 0.4$, designated as proton contamination.

The validity of such event characterisations was confirmed using the neutron yield from the calorimeter and the ionization (dE/dx) losses measured in the spectrometer. These distributions were studied for positively- and negatively-charged events after the calorimeter selection and compared to the corresponding distributions derived from the entire set of data for negatively charged (mostly electrons) and positively charged (overwhelmingly proton) events. A higher neutron yield is expected in hadronic interactions in the calorimeter, especially at energies greater than 10 GeV. Competing density and logarithmic rise effects for dE/dx losses in the silicon detectors of the spectrometer yield different dE/dx distributions for electrons and protons between 10 and 25 GeV. This is a particularly important check, as the spectrometer information is independent of the calorimeter and can be used to rule out proton interactions resulting in (e.g.) π^0 production in the topmost calorimeter planes. The π^0 will decay to two photons that can generate electromagnetic showers in the calorimeter. A Kolmogorov-Smirnov test showed that the distributions for events characterised as positrons (protons) were statistically compatible, thereby rejecting the null hypothesis at 5% level, with the corresponding negatively- (positively-) charged distributions.

The event selection methodology was further validated using particle beam data collected prior to launch[26] and data generated using the PAMELA Collaboration's official simulation program that reproduces the entire PAMELA apparatus, including the spectrometer magnetic field and the pressure vessel. Similar conclusions were derived from cosmic-ray data collected by the CAPRICE98 balloon-borne experiment[27]. This apparatus was equipped

with a similar but thinner (7 radiation lengths) silicon-tungsten calorimeter. A gas-RICH detector allowed background-free samples of protons (i.e. no positron contamination) to be selected up to 50 GeV. Within the limits of available statistics, the reconstructed proton and electron/positron lateral energy distributions were fully consistent with those obtained with the PAMELA calorimeter.

BACKGROUND ESTIMATION

While the distribution shown in Fig. 1 presents a clear positron signature, the residual proton background distribution must be quantified. This distribution was obtained using the flight calorimeter data. There was no dependence on simulations. The total calorimeter depth of 22 detector planes was divided in two non-mutually exclusive parts: an upper part comprising planes 1-20, and a lower part comprising planes 3-22. Calorimeter variables (e.g. total detected energy, and lateral shower spread) were evaluated for both parts. Electrons and positrons can be identified in the upper part of the calorimeter using the total detected energy and the starting point of the shower. The positron component in positively charged events can be significantly reduced by selecting particles that do not interact in the first 2 planes (only 2% of electrons and positrons with rigidities greater than 1.5 GV pass this condition). This results in a nearly pure sample of protons entering the lower part of the calorimeter (planes 3-22). The procedure was validated using simulations. As an example Fig. 2a shows the energy fraction variable, \mathcal{F} , for negatively charged particles in the rigidity range 28–42 GV selected as electrons in the upper half of the calorimeter. Panels (b) and (c) show the \mathcal{F} distributions for positively-charged particles obtained for the lower (upper) part of the calorimeter, i.e. protons (protons and positrons). The distributions in panels (a) and (b) are clearly different while panel (c) shows a mixture of the two distributions, which strongly supports the positron interpretation for the electron-like \mathcal{F} distribution in the sample of positively charged events. A parametric bootstrap analysis with maximum likelihood fitting was performed on the distributions shown in Fig. 2 for a number of rigidity intervals, and the numbers of detected electrons, positrons, and contaminating protons were obtained. As a cross-check, a non-parametric statistic analysis, using Kolmogorov-Smirnov tests, were applied to electron, positron and proton distributions. The results (numbers of identified positrons and protons) were statistically consistent (well within one standard

deviation) with those obtained using the parametric method.

THE POSITRON FRACTION

The results presented here are based on the data-set collected by PAMELA between July 2006 and February 2008. More than 10^9 triggers were accumulated during a total acquisition time of approximately 500 days. From these triggered events 151,672 electrons and 9,430 positrons were identified in the energy interval 1.5 - 100 GeV. Results are presented as a positron fraction and are shown in Table I. The detection efficiencies for electrons and positrons are assumed to cancel since the physical processes that these species undergo in the PAMELA detectors can be assumed to be identical across the energy range of interest. Possible bias arising from a sign-of-charge dependence on the acceptance due to the spectrometer magnetic field configuration and East-West effects caused by the Earth's magnetic field were excluded as follows. Effects due to the spectrometer magnetic field were studied using the PAMELA Collaboration's simulation software. No significant difference was found between the electron and positron detection efficiency above 1 GV. East-West effects as well as contamination from re-entrant albedo particles (secondary particles produced by cosmic-rays interacting with the Earth's atmosphere that are scattered upward but lack sufficient energy to leave the Earth's magnetic field and re-enter the atmosphere in the opposite hemisphere but at a similar magnetic latitude) are significant around and below the lowest permitted rigidity for a charged cosmic-ray to reach the Earth from infinite distance, known as the geomagnetic cut-off. The geomagnetic cut-off for the PAMELA orbit varies from less than 100 MV for the highest orbital latitudes to approximately 15 GV for equatorial regions. In this work, only events with a measured rigidity exceeding the estimated vertical (PAMELA z-axis) geomagnetic cut-off by a factor of 1.3 were considered. This reduced East-West effects and re-entrant particle contamination to a negligible amount. The vertical geomagnetic cut-off was determined following the Størmer formalism (e.g.[28]) on an event-by-event basis and using orbital parameters reconstructed at a rate of 1 Hz.

Fig. 3 shows the positron fraction measured by the PAMELA experiment compared with other recent experimental data. The PAMELA data covers the energy range 1.5 - 100 GeV, with significantly higher statistics than other measurements. Two features are clearly visible in the data. At low energies (below 5 GeV) the PAMELA results are systematically lower

than data collected during the 1990's and at high energies (above 10 GeV) the PAMELA results show that the positron fraction increases significantly with energy.

OBSERVATION OF CHARGE-SIGN DEPENDENT SOLAR MODULATION EFFECTS

The solar wind modifies the energy spectra of cosmic-rays within the solar system. This effect is called solar modulation and can have a significant effect on cosmic-rays with energies less than about 10 GeV. The amount of solar modulation depends on solar activity, which has an approximately sinusoidal time dependence and is most evident at solar maximum, when the low energy cosmic ray flux is at a minimum. The peak-to-peak period is 11 years, but a complete 'solar cycle' is 22 years long since at each maximum the polarity of the solar magnetic field reverses. The low energy difference between the PAMELA results and those from CAPRICE94[32], HEAT95[31] and AMS-01[33] are interpreted as a consequence of solar modulation effects. These older results were collected during the previous solar cycle which favored positively-charged particles due to the solar polarity. Indications that solar modulation effects depend on the cosmic-ray sign-of-charge have been clearly seen in the antiproton-to-proton flux ratio measured before and after the most recent (2000) reversal of the solar magnetic field by a series of flights of the BESS balloon-borne experiment[36]. In this case, solar modulation effects were seen mostly at low rigidities (<2 GV), and during a period of maximum solar activity. During the period of solar minimum corresponding to PAMELA data taking, solar modulation becomes negligible in the BESS data-set. The low cosmic-ray antiproton flux limits a detailed study of this effect. In the PAMELA data-set, charge dependent solar modulation effects on electrons and positrons are evident up to nearly 5 GV, even during the current period of minimum solar activity. Contemporary models interpret charge-sign dependent modulation in the heliosphere as being due to gradient, curvature and current sheet drift effects[37]. Drift effects are at their largest during solar minimum conditions and mostly affect low mass particles such as electrons and positrons, with electrons being favoured in the current solar cycle. A balloon-borne experiment which flew in June 2006 has also observed a low positron fraction[35] at low energies, but with large statistical uncertainties.

THE HIGH ENERGY ANOMALY

Between 5-10 GeV, the PAMELA positron fraction is compatible with other measurements. Previously, the HEAT experiment[38] claimed a structure in the positron fraction between 6 and 10 GeV but this is not confirmed by the PAMELA data.

Above 10 GeV, the PAMELA results clearly show that the positron fraction increases significantly with energy. Fig. 4 shows the PAMELA positron fraction compared to a calculation[39] for the secondary production of positrons during the propagation of cosmic-ray nuclei in the galaxy without reacceleration processes. While this calculation is widely used, it does not account for uncertainties related to the production of secondary positrons and electrons. Uncertainties arise due to incomplete knowledge of (a) the primary cosmic-ray nuclei spectra, (b) modelling of interaction cross-sections and (c) modelling of cosmic-ray propagation in the galaxy. Uncertainties on the primary electron spectrum are also relevant, but since the electron injection spectrum at source is expected to have a power law index of approximately -2 (e.g.[40]) and be equal to that of protons (e.g.[41]) up to about 1 TeV, the positron fraction is expected to fall as a smooth function of increasing energy if secondary production dominates.

A rise in the positron fraction at high energy has been postulated for the annihilation of dark matter particles in the galactic halo[5, 6, 7, 8, 9, 10, 11]. The production of positrons through pair production processes in the magnetosphere of near-by pulsars would also yield a similar positron signature[16, 17, 18, 19, 20]. We note, however, that none of the published models fit our data well and the reason for the rise remains unexplained.

CONCLUSIONS AND FUTURE PROSPECTS

We have presented the cosmic-ray positron fraction over a wide energy range, including the highest energy ever achieved, and with more than an order of magnitude increase in statistics over previous experiments. Our results clearly show an increase in the positron abundance at high energy that cannot be understood by standard models describing the secondary production of cosmic-rays. Either a significant modification in the acceleration and propagation models for cosmic-rays is needed, or a primary component is present. There are several interesting candidates for a primary component, including the annihilation of

dark matter particles in the vicinity of our galaxy. There may also be a contribution from near-by astrophysical sources, such as pulsars. The low energy data show a significant charge-sign dependence for solar modulation and this is the most statistically significant observation of this effect to date. The data are sufficiently precise to allow models of the heliosphere to be tuned. PAMELA will continue to collect data until at least December 2009. The corresponding increase in statistics will allow higher energies to be studied (up to the expected spillover limit at approximately 300 GeV). These measurements are likely to be important when determining the origin of the observed rise, especially if an edge is seen in positron fraction as expected in many dark matter based models. If, on the other hand, the positron fraction is dominated by a single near-by source, there may be an anisotropy in the arrival direction of the electrons and positrons[20]. Work is in progress to reconstruct the positron fraction down to an energy of 100 MeV, permitting more extensive tests of solar modulation models.

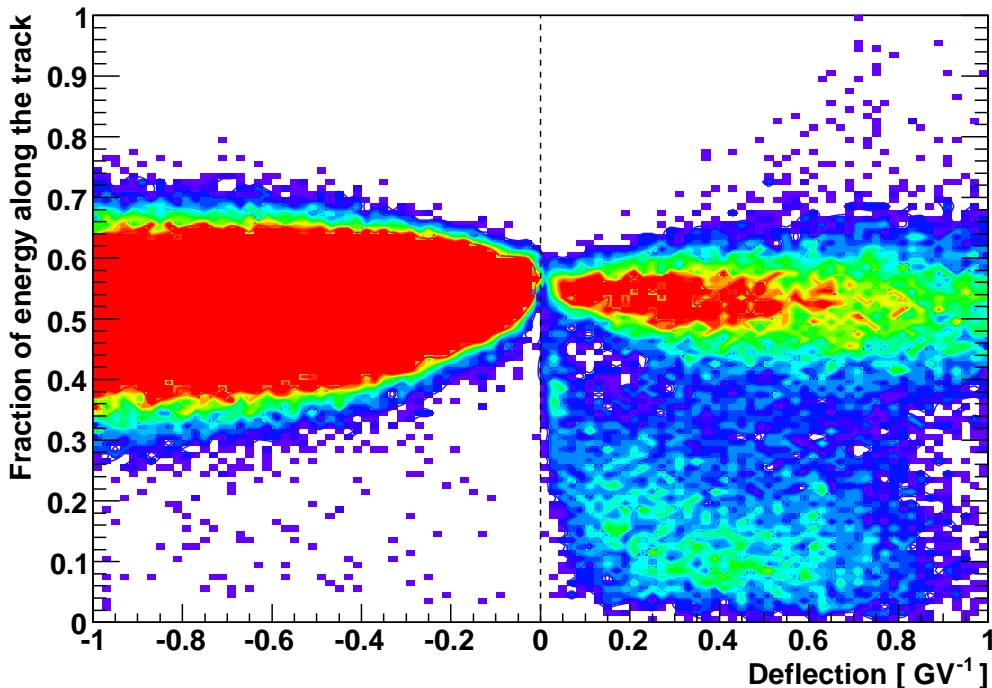


FIG. 1: **Calorimeter energy fraction \mathcal{F}** . The fraction of calorimeter energy deposited inside a cylinder of radius 0.3 Molière radii, as a function of deflection. The axis of the cylinder is defined by extrapolating the particle track reconstructed by the spectrometer.

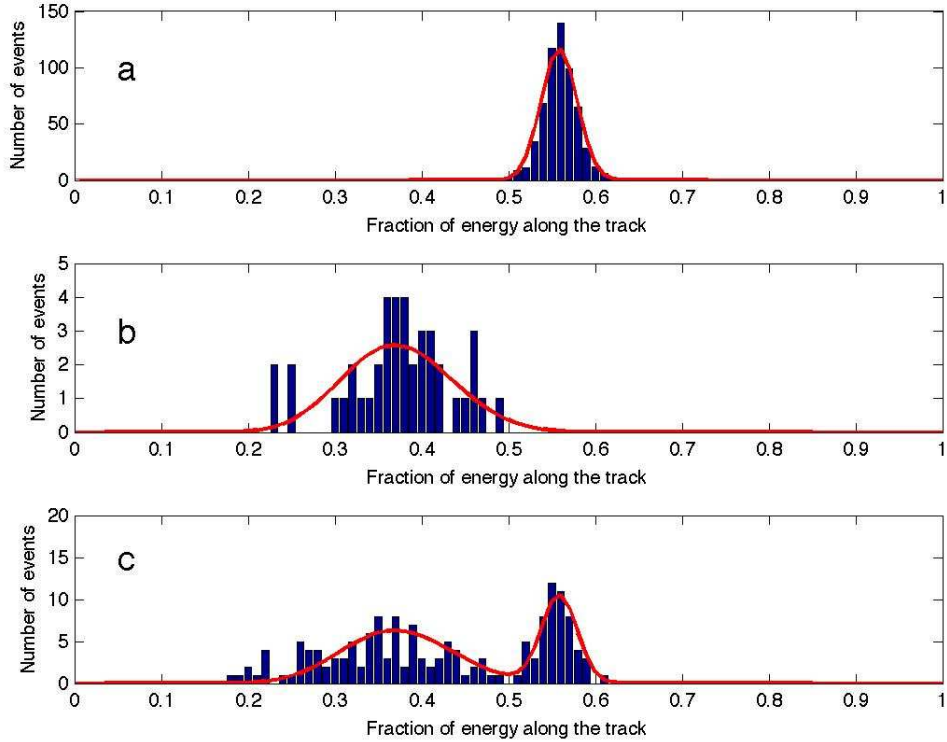


FIG. 2: **Calorimeter energy fraction \mathcal{F} : 28–42 GV.** Panel **a** shows the distribution of the energy fraction for negatively charged particles, selected as electrons in the upper part of the calorimeter. Panel **b** shows the same distribution for positively charged particles selected as protons in the bottom part of the calorimeter. Panel **c** shows positively charged particles, selected in the upper part of the calorimeter, i.e. protons and positrons.

METHODS

The PAMELA apparatus.

The PAMELA apparatus is inserted inside a pressurized container (2 mm aluminum window) attached to the Russian Resurs-DK1 satellite. The apparatus, approximately 120 cm tall and with a mass of about 450 kg, can be seen in fig. 5, which shows a 68 GeV positively-charged particle selected as a positron. It comprises the following detector systems (from top to bottom): a time-of-flight system (ToF (S1, S2, S3)); a magnetic spectrometer; an anticoincidence system (AC (CARD, CAT, CAS)); an electromagnetic imaging calorimeter;

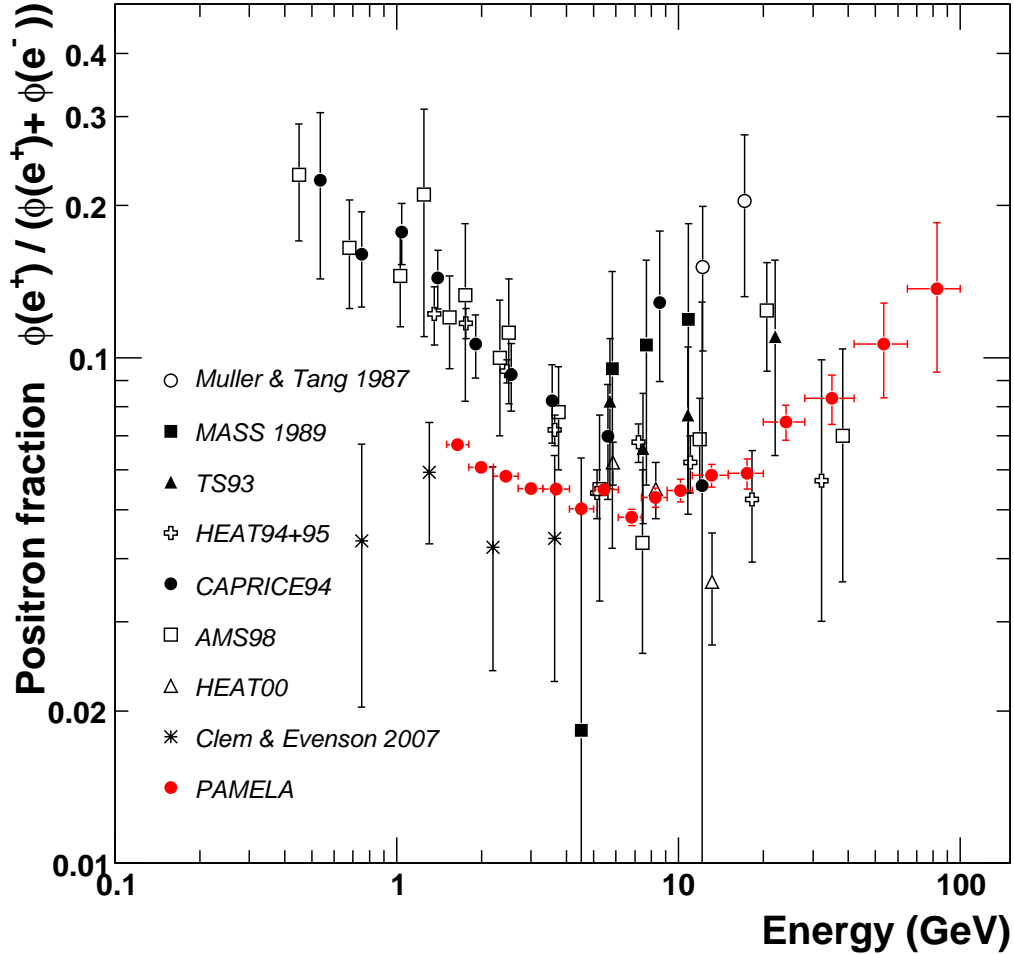


FIG. 3: **PAMELA positron fraction with other experimental data.** The positron fraction measured by the PAMELA experiment compared with other recent experimental data[24, 29, 30, 31, 32, 33, 34, 35]. One standard deviation error bars are shown. If not visible, they lie inside the data points.

a shower tail catcher scintillator (S4) and a neutron detector. The ToF system provides a fast signal for triggering the data acquisition and measures the time-of-flight and ionization energy losses (dE/dx) of traversing particles. It also allows down-going particles to be reliably identified. Multiple tracks, produced in interactions above the spectrometer, were rejected by requiring that only one strip of the top ToF scintillator (S1 and S2) layers registered an energy deposition ('hit'). Similarly no hits were permitted in either top scintillators of the AC system (CARD and CAT). The central part of the PAMELA apparatus is

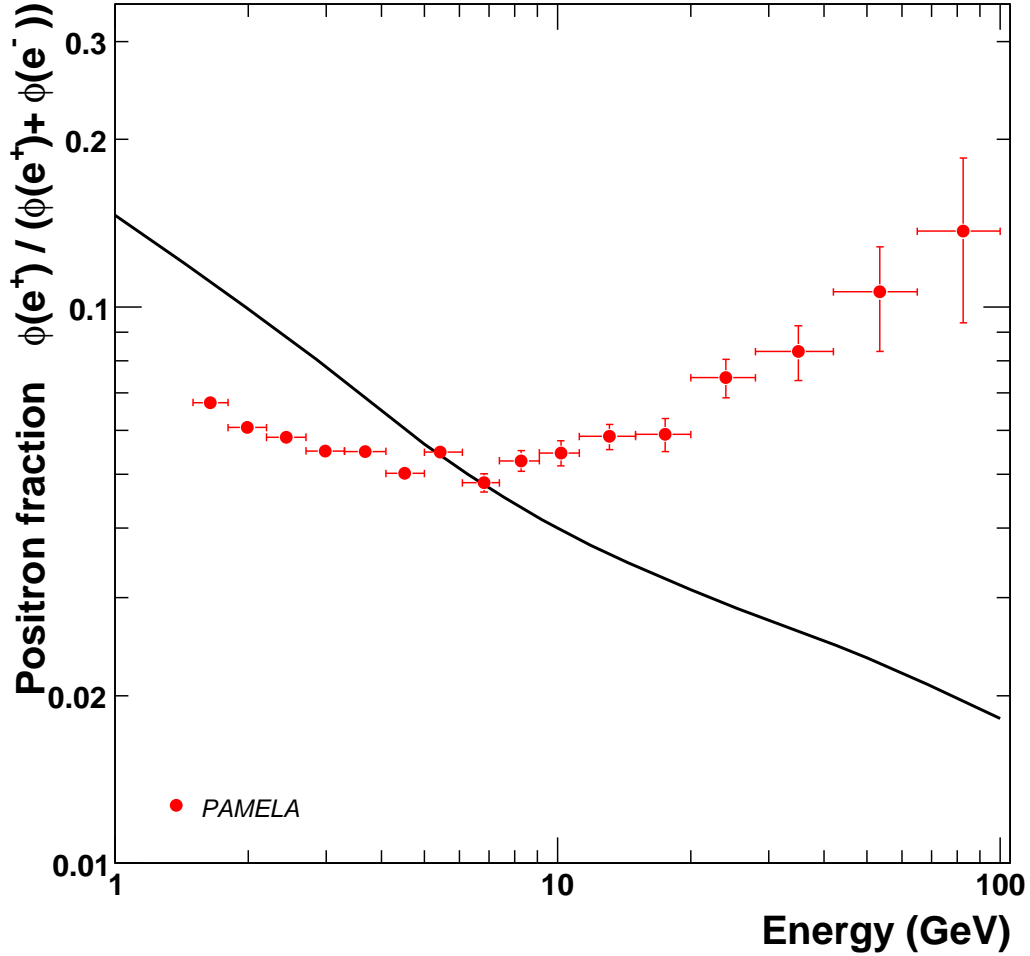


FIG. 4: **PAMELA positron fraction with theoretical models.** The PAMELA positron fraction compared with theoretical model. The solid line shows a calculation by Moskalenko & Strong[39] for pure secondary production of positrons during the propagation of cosmic-rays in the galaxy. One standard deviation error bars are shown. If not visible, they lie inside the data points.

a magnetic spectrometer consisting of a 0.43 T permanent magnet and a silicon microstrip tracking system. The spectrometer measures the rigidity of charged particles through their deflection in the magnetic field. During flight the spatial resolution is observed to be $3\mu\text{m}$ corresponding to a maximum detectable rigidity (MDR) exceeding 1 TV. Due to the finite spatial resolution in the spectrometer, high rigidity (low deflection) electrons may 'spill over' into the positron sample (and vice-versa) if assigned the wrong sign-of-curvature. This

spillover background was eliminated by imposing a set of strict selection criteria on the quality of the fitted tracks. The spillover limit for positrons is estimated from flight data and simulation to be approximately 300 GeV, as expected from particle beam tests. The dE/dx losses measured in S1 and the silicon layers of the magnetic spectrometer were used to select minimum ionizing singly charged particles (mip) by requiring the measured dE/dx to be less than twice that expected from a mip. The sampling calorimeter comprises 44 silicon sensor planes interleaved with 22 plates of tungsten absorber. Each tungsten layer has a thickness of 0.26 cm corresponding to 0.74 radiation lengths. Positrons (electrons) can be selected from a background of protons (antiprotons) by studying the properties of the energy deposition and interaction topology. A high dynamic-range scintillator system and a neutron detector are mounted under the calorimeter at the bottom of the apparatus.

Statistical methods.

For each energy interval, the distribution of the calorimeter energy fraction (\mathcal{F}) for positively-charged particles (e.g. Fig. 2c) was expressed as mixture distribution[43] of positrons (i.e. signal, electrons as in Fig. 2a) and protons (background, e.g. Fig. 2b):

$$f(\mathcal{F}) = p \cdot g_1(\mathcal{F}; q_1) + (1 - p) \cdot g_2(\mathcal{F}; q_2) \quad (1)$$

where the parameter p gives the mixture proportion; $g_1(\mathcal{F}; q_1)$ and $g_2(\mathcal{F}; q_2)$ are the probability density functions (p.d.f.) for positrons/electrons and protons, respectively. The p.d.f.'s g_1 and g_2 were determined by analysing two samples of pure electrons (Fig. 2a) and protons (Fig. 2b) in the same energy range. We used a Beta distribution for both the electron/positron signal g_1 and for the proton background g_2 . In both cases parameter sets q_1 and q_2 were determined from a maximum likelihood fit.

The mixture proportion p was estimated by means of a bootstrap procedure [44] followed by the maximum likelihood method. As first step, the experimental distribution was re-sampled, by means of a bootstrap procedure, $N = 1000$ times. For each re-sample i ($i = 1, \dots, N$) we estimated the unknown parameter p_i by means of an un-binned maximum likelihood analysis. The likelihood is defined by:

$$L_i = \prod_{j=1}^K [p_i g_1(\mathcal{F}_j; q_1) + (1 - p_i) g_2(\mathcal{F}_j; q_2)]$$

where K is the total number of positive particles (e.g. Fig. 2c) and $j=1, \dots, K$.

The best fit point for p_i corresponds to the maximum L_i . Therefore as a result we obtained from eq. 1 N estimations of the number of positrons candidates (n_i^+). Then, the final number of positron candidates was obtained as

$$n = \frac{1}{N} \sum_{i=1}^N n_i^+$$

We also estimated the α -level confidence interval including all the values of n_i^+ between the $\alpha/2$ and $1 - \alpha/2$ percentiles of the n_i^+ distribution. We chose one standard deviation as the confidence interval.

An alternative non-parametric statistical method to evaluate the proton background required the construction of a test sample. The test sample was built by combining the proton sample with a weight w and the electron sample with a weight $1 - w$, with $w \in (0, 1)$. The value of w is chosen by minimizing the Kolmogorov-Smirnov distance between the positive sample and the test one. Furthermore, a Mann-Whitney test is applied around the positron peak in order to check if the two sets are compatible. After the normalization of the test sample, the proton background is found by counting only the proton events (with their own weight) inside the positron selection region. The calculation of the confidence interval is based on the likelihood ratio test[45], by considering proper probability models for the positron signal, the proton background, the selection efficiency and the weight w .

ACKNOWLEDGMENTS

We would like to thank D. Marinucci for helpful discuss concerning the statistical methods, D. Müller and S. Swordy and their group at University of Chicago, G. Bellettini and G. Chiarelli for helpful discussion on the data analysis and L. Bergström for useful comments on the interpretation of our results. We acknowledge support from The Italian Space Agency (ASI), Deutsches Zentrum für Luft- und Raumfahrt (DLR), The Swedish National Space Board, The Swedish Research Council, The Russian Space Agency (Roscosmos) and The Russian Foundation for Basic Research.

Competing Interests The authors declare that they have no competing financial interests.

Correspondence Correspondence and requests for materials should be addressed to P.P. (email: Piergiorgio.Picozza@roma2.infn.it).

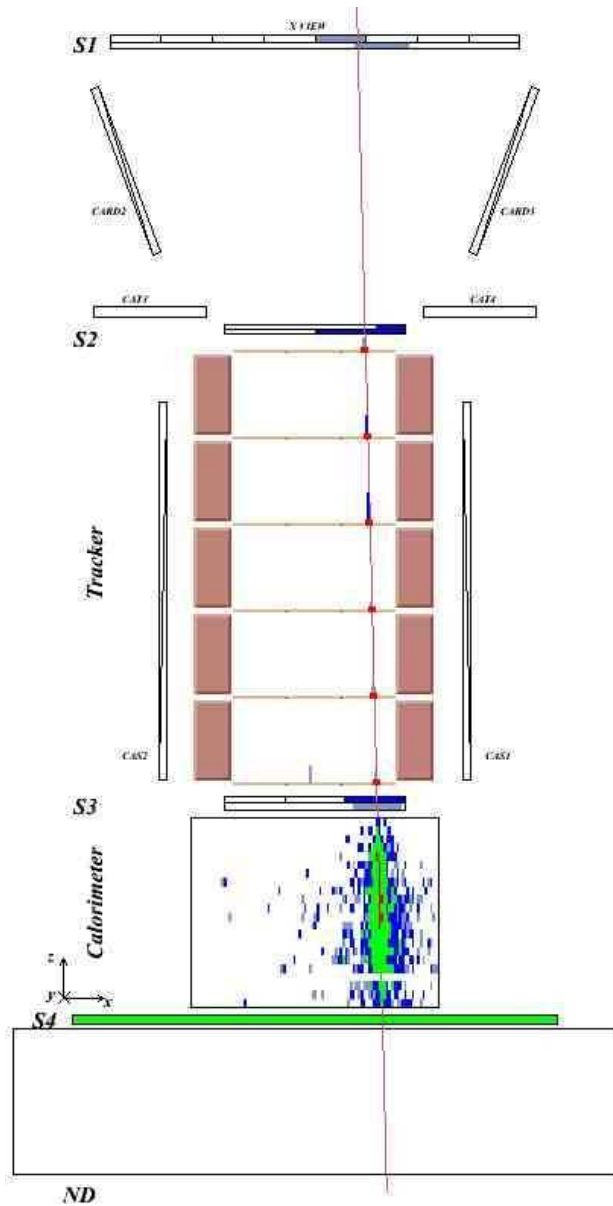


FIG. 5: **Positron Event display.** A 68 GeV positively-charged particle selected as positron. The bending (x) view is shown. The signals as detected by PAMELA detectors are shown along with the particle trajectory (solid line) reconstructed by the fitting procedure of the tracking system. The calorimeter shows the typical signature of an electromagnetic shower (plane 19 of the calorimeter x-view was malfunctioning).

TABLE I: Summary of positron fraction results. The errors are one standard deviation.

Rigidity at spectrometer	Mean Kinetic Energy at top of payload	Extrapolated $\frac{\phi(e^+)}{\phi(e^+)+\phi(e^-)}$ at top of payload
GV	GeV	
1.5 – 1.8	1.64	$(0.0673^{+0.0014}_{-0.0013})$
1.8 – 2.2	1.99	(0.0607 ± 0.0012)
2.2 – 2.7	2.44	(0.0583 ± 0.0011)
2.7 – 3.3	2.99	(0.0551 ± 0.0012)
3.3 – 4.1	3.68	(0.0550 ± 0.0012)
4.1 – 5.0	4.52	(0.0502 ± 0.0014)
5.0 – 6.1	5.43	(0.0548 ± 0.0016)
6.1 – 7.4	6.83	(0.0483 ± 0.0018)
7.4 – 9.1	8.28	(0.0529 ± 0.0023)
9.1 – 11.2	10.17	$(0.0546^{+0.0029}_{-0.0028})$
11.2 – 15.0	13.11	$(0.0585^{+0.0030}_{-0.0031})$
15.0 – 20.0	17.52	$(0.0590^{+0.0040}_{-0.0041})$
20.0 – 28.0	24.02	(0.0746 ± 0.0059)
28.0 – 42.0	35.01	(0.0831 ± 0.0093)
42.0 – 65.0	53.52	$(0.106^{+0.022}_{-0.023})$
65.0 – 100.0	82.55	$(0.137^{+0.048}_{-0.043})$

-
- [1] Komatsu, E. *et al.* Five-year wilkinson microwave anisotropy probe (WMAP) observations: cosmological interpretation. Accepted for publication in ApJS (2008); preprint at arXiv:0803.0547v2 [astro-ph].
- [2] Jungman, G., Kamionkowski, M. & Griest, K. Supersymmetric dark matter. Phys. Rept. **267**, 195-373 (1996).
- [3] Cheng, H. C., Feng, J. L. & Matchev, K. T. Kaluza-Klein dark matter. Phys. Rev. Lett. **89**, 211301-211304 (2002).

- [4] Buchmuller, W., Covi, L., Hamaguchi, K., Ibarra, A. & Yanagida, T. Gravitino dark matter in R-parity breaking vacua. *JHEP* **0703**, 037 (2007).
- [5] Tylka, A. J. Cosmic ray positrons from annihilation of weakly interacting massive particles in the galaxy. *Phys. Rev. Lett.* **63**, 840-843 (1989). [Erratum-ibid. **63**, 1658 (1989)]
- [6] Turner, M. S. & Wilczek, F. Positron line radiation from halo WIMP annihilations as a dark matter signature. *Phys. Rev. D* **42**, 1001-1007 (1990).
- [7] Kamionkowski, M. & Turner, E. M. Distinctive positrons feature from particle dark-matter annihilations in the galactic halo. *Phys. Rev. D* **43**, 1774-1780 (1991).
- [8] Kane, G. L., Wang, L. L. & Wells, J. D. Supersymmetry and the positron excess in cosmic rays. *Phys. Rev. D* **65**, 057701-057704 (2002).
- [9] Baltz, E. A., Edsjo, J., Freese, K. & Gondolo, P. The cosmic ray positron excess and neutralino dark matter. *Phys. Rev. D* **65**, 063511-063520 (2002)
- [10] Baltz, E. A. & Bergström, L. Detection of leptonic dark matter. *Phys. Rev. D* **67**, 043516-043522 (2003).
- [11] Bertone, G., Hooper, D. & Silk, J. Particle dark matter: Evidence, candidates and constraints. *Phys. Rept.* **405**, 279-390 (2005).
- [12] Hooper, D. & Profumo, S. Dark matter and collider phenomenology of universal extra dimensions. *Phys. Rept.* **453**, 29-115 (2007).
- [13] Ibarra, A. & Tran, D. Antimatter Signatures of Gravitino Dark Matter Decay. *JCAP* **0807**, 002 (2008).
- [14] Bottino, A., Donato, F., Fornengo, N. & Scopel, S. Indirect signals from light neutralinos in supersymmetric models without gaugino mass unification. *Phys. Rev. D* **70**, 015005-0150019 (2004).
- [15] Adriani, O. *et al.* A new measurement of the antiproton-to-proton flux ratio up to 100 GeV in the cosmic radiation. submitted to *Phys. Rev. Lett.* (2008).
- [16] Harding, A. K. & Ramaty, R. The pulsar contribution to galactic cosmic-ray positrons. *Proc. 20th ICRC, Moscow* **2**, 92-95 (1987).
- [17] Atoian, A. M., Aharonian, F. A., & Volk, H. J. Electrons and positrons in the galactic cosmic-rays. *Phys. Rev. D* **52**, 3265-3275 (1995).
- [18] Chi, X., Cheng, K. S. & Young, E. C. M. Pulsar-wind origin of cosmic-ray positrons. *Astrophys. J.* **459**, L83-L86 (1996).

- [19] Grimani, C. Pulsar birthrate set by cosmic-ray positron observations. *Astron. Astrophys.* **418**, 649-653 (2004).
- [20] Büsching, I., de Jager, O. C., Potgieter, M. S. & Venter, C. A cosmic-ray positron anisotropy due to two middle-aged, nearby pulsars? *Astrophys. J.* **78**, L39-L42 (2008).
- [21] Müller, D. Cosmic-ray electrons and positrons. *Adv. in Space Res.* **27**, 659-668 (2001).
- [22] Barwick, S. W. *et al.* Cosmic-ray positrons at high energies: A new measurement. *Phys. Rev. Lett.* **75**, 390-393 (1995).
- [23] Golden, R. L. *et al.* Measurement of the positron to electron ratio in the cosmic rays above 5 GeV. *Astrophys. J.* **457**, L103-L106 (1996).
- [24] Gast, H., Olzem, J. & Schael, S. Indirect dark matter search: Cosmic positron fraction measurement from 1 GeV to 50 GeV with AMS-01. *Proc. XLIIst Rencontres de Moriond, Electroweak Interactions and Unified Theories*, 421-428 (2006).
- [25] Picozza, P. *et al.* PAMELA - A payload for antimatter matter exploration and light-nuclei astrophysics. *Astropart. Phys.* **27**, 296-315 (2007).
- [26] Boezio, M. *et al.* The electron-hadron separation performance of the PAMELA electromagnetic calorimeter. *Astropart. Phys.* **26**, 111-118 (2006).
- [27] Boezio, M. *et al.* The cosmic-ray antiproton flux between 3 and 49 GeV. *Astrophys. J.* **561**, 787-799 (2001).
- [28] Hopper, V. D. *Cosmic radiation and high energy interactions* (Academic Press, London, 1964).
- [29] Müller, D. & Tang, K. K. Cosmic-ray positrons from 10 to 20 GeV - A balloon-borne measurement using the geomagnetic east-west asymmetry. *Astrophys. J.* **312**, 183-194 (1987).
- [30] Golden, R. L. *et al.* Observations of cosmic-ray electrons and positrons using an imaging calorimeter. *Astrophys. J.* **436**, 769-775 (1994).
- [31] Barwick, S. W. *et al.* Measurements of the cosmic-ray positron fraction from 1 to 50 GeV. *Astrophys. J.* **482**, L191-194 (1997).
- [32] Boezio, M. *et al.* The cosmic-ray electron and positron spectra measured at 1 AU during solar minimum activity. *Astrophys. J.* **532**, 653-669 (2000).
- [33] Alcaraz, J. *et al.* Leptons in near earth orbit. *Phys. Lett. B* **484**, 10-22 (2000).
- [34] Beatty, J. J. *et al.* New measurement of the cosmic-ray positron fraction from 5 to 15 GeV. *Phys. Rev. Lett.* **93**, 241102-241105 (2004);
- [35] Clem, J. & Evenson, P. Cosmic ray positron fraction observations during the A-magnetic solar

- minimum. Proc. 30th ICRC, Merida (2007).
- [36] Asaoka, Y. *et al.*, Measurements of cosmic-ray low-energy antiproton and proton spectra in a transient period of the solar field reversal. *Phys. Rev. Lett.* **88**, 051101-051104 (2002).
- [37] Potgieter, M. S., Burger, R. A. & Ferreira, S. E. S. Modulation of cosmic rays in the heliosphere from solar minimum to maximum: a theoretical perspective. *Space Sci. Rev.* **97**, 295-307 (2001).
- [38] Coutu, S. *et al.* Cosmic-ray positrons: are there primary sources? *Astropart. Phys.* **11**, 429-435 (1999).
- [39] Moskalenko, I. V. & Strong, A. W. Production and propagation of cosmic-ray positrons and electrons. *Astrophys. J.* **493**, 694-707 (1998).
- [40] Aharonian, F. *et al.* First detection of a VHE gamma-ray spectral maximum from a cosmic source: HESS discovery of the Vela X nebula. *Astron. Astrophys.* **448**, L43-L47 (2006).
- [41] Berezhko, E. G., Ksenofontov, L. T. & Völk, H. J. Emission of SN 1006 produced by accelerated cosmic rays. *Astron. Astrophys.* **395**, 943-953 (2002).
- [42] Zhang, L. & Cheng, K. S. Cosmic-ray positrons from mature gamma-ray pulsars. *Astron. Astrophys.* **368**, 1063-1070 (2001).
- [43] Everit, B.S. and Hand, D.J. *Finite Mixture Distributions*. Chapman and Hall (1981).
- [44] Efron, B. Bootstrap methods: another look at the jackknife. *Ann. Stat.* **7**, 1-26 (1979).
- [45] Rolke, W. A., Lopez, A. M. & Conrad, J. Limits and confidence intervals in the presence of nuisance parameters. *Nucl. Instrum. Meth. A* **551**, 493-503 (2005)